The magnitudes of the bond length changes are comparable with those (~0.03 Å) calculated by Frank-Condon analyses[24] to take place in $[MnO_4]^-$,[24,25] $[MnO_4]^{2-}$,[7] $[MoS_4]^{2-}$,[8] and $[WS_4]^{2-}$,[9] on exciting the highest nonbonding electron to the lowest antibonding orbital.

Acknowledgment. This work is made possible by Grant NSF CHE 88-06775 from the National Science Foundation (K.S.S., J.I.Z.). J.I.Z. also gratefully acknowledges a fellowship from the John Simon Guggenheim Memorial Foundation, which was held in part at University College London.

(24) Clark, R. J. H.; Dines, T. J. *Angew. Chem., Int. Ed.* **1986**, *25*, 131.
(25) Clark, R. J. H.; Stewart, B. *J. Am. Chem. Soc.* **1981**, *103*, 6593.

Electronic Absorption and MCD Spectra of $M_2(TMB)_4^{2+}$, M = Rh and Ir. A Valence-Bond Description of the Upper Electronic Excited States

David C. Smith,† Vincent M. Miskowski,† W. Roy Mason,‡ and Harry B. Gray*,†

Contribution No. 7970 from the Arthur Amos Noyes Laboratory, California Institute of Technology, Pasadena, California 91125, and Department of Chemistry, Northern Illinois University, DeKalb, Illinois 60115. *Received August 7, 1989*

Abstract: Electronic absorption and magnetic circular dichroism (MCD) spectra of $Rh_2(TMB)_4^{2+}$ and $Ir_2(TMB)_4^{2+}$ are reported along with polarized single-crystal absorption spectra of $[Ir_2(TMB)_4][B(C_6H_5)_4]_2 \cdot CH_3C_6H_5$ (TMB = 2,5-diisocyano-2,5-dimethylhexane). Interpretation of the spectra is based on a valence-bond model that accommodates highly perturbed dimer transitions as well as monomer-like dimer excitations. In this model, half of the dimer electronic excited states possess ionic character; these states involve metal-to-metal charge transfer (MMCT). The intense absorptions of $Ir_2(TMB)_4^{2+}$ are assigned as follows: $d\sigma^* \rightarrow p\sigma$ [$A_{1g}(^1A_{1g}) \rightarrow E_u(^3A_{2u})$ and $A_{2u}(^1A_{2u})$] at 820 and 635 nm; $d_{xz,yz} \rightarrow p_z$ [$A_{1g}(^1A_{1g}) \rightarrow E_u$, $A_{2u}(^3E_u)$ and $E_u(^1E_u)$] at 373, 331, and 320 nm; and $d_{xy} \rightarrow p_z$ [$A_{1g}(^1A_{1g}) \rightarrow E_u(^3B_{1u})$] at 304 nm. Several weak features are observed to lower energy of the $A_{1g}(^1A_{1g}) \rightarrow E_u(^3A_{2u})$ band. The most prominent of the weak features (~430 nm) is assigned to the transition to $^1A_{1g}$ (a single-center $d_{z^2} \rightarrow p_z$ excitation). High-energy features ($\lambda < 300$ nm) in the spectra of $Rh_2(TMB)_4^{2+}$ and $Ir_2(TMB)_4^{2+}$ are assigned to MMCT arising from $d_{xz,yz} \rightarrow p_z$ excitations.

The electronic spectra of face-to-face, metal-metal-bonded d^8-d^8 complexes have been extensively discussed on the basis of a molecular orbital (MO) model.[1-10] In this picture, the metal-based d_{z^2} (filled) and p_z (empty) orbitals each interact strongly to produce pairs of bonding and antibonding orbitals. Configuration interaction between the empty and filled sets (which might alternatively be visualized as dative d-p bonding) provides the weak ground-state bond, while the lowest energy singlet and triplet excited states, derived from the $d\sigma^* \rightarrow p\sigma$ one-electron transition, are strongly stabilized relative to their respective monomer $d_{z^2} \rightarrow p_z$ states.

While this picture accounts for some important aspects of the metal-metal interaction, it also has been noted that several monomer d → p excitations are only slightly perturbed in the d^8-d^8 complexes.[1] This observation and the rather long metal-metal bonds (3.1-3.3 Å)[11,12] suggest that d^8-d^8 species should be examined in terms of valence-bond (VB) theory.

In addition to beginning such an examination, and to complement earlier investigations of rhodium complexes ($Rh_2(TMB)_4^{2+}$, TMB = 2,5-diisocyano-2,5-dimethylhexane; $Rh_2b_4^{2+}$, b = 1,3-diisocyanopropane), we undertook a detailed study of the electronic spectrum of $Ir_2(TMB)_4^{2+}$. A change in the metal from rhodium to iridium should perturb the electronic structure, thereby altering the characteristic d^8-d^8 electronic spectrum and allowing us to test key aspects of the MO and VB models. We report here the electronic absorption and magnetic circular dichroism (MCD) spectra of $Rh_2(TMB)_4^{2+}$ and $Ir_2(TMB)_4^{2+}$ along with polarized single-crystal absorption spectra of $[Ir_2(TMB)_4][B(C_6H_5)_4]_2 \cdot CH_3C_6H_5$.

Experimental Section

All synthetic procedures were carried out with standard Schlenk techniques unless otherwise specified. Tetrahydrofuran (THF) was distilled from CaH_2 prior to use. Other solvents were taken from freshly opened bottles and were not purified further, except as noted. All solvents were Schlenk degassed prior to use. Standard procedures were used to prepare 2,5-diisocyano-2,5-dimethylhexane (TMB),[11] $[Ir_2(TMB)_4][B(C_6H_5)_4]_2$,[13] $[Ir(COD)Cl]_2$ (COD = 1,5-cyclooctadiene),[14] $[Ir(COD)_2]BF_4$,[15] and $[Rh_2(TMB)_4](PF_6)_2$.[11] The literature preparation of Ir(COD)(acac) (acac = acetylacetone),[16] a precursor to $[Ir(COD)_2]BF_4$, was modified as noted below. All other chemicals were reagent grade or comparable quality and were used as received. The ^1H NMR spectra were obtained on a 400-MHz JNM-GX400 FT NMR spectrometer.

* To whom correspondence should be addressed.
† California Institute of Technology.
‡ Northern Illinois University.

(1) Rice, S. F.; Miskowski, V. M.; Gray, H. B. *Inorg. Chem.* **1988**, *27*, 4704-4708.
(2) Stiegman, A. E.; Rice, S. F.; Gray, H. B.; Miskowski, V. M. *Inorg. Chem.* **1987**, *26*, 1112-1116.
(3) Isci, H.; Mason, W. R. *Inorg. Chem.* **1985**, *24*, 1761-1765.
(4) Rodman, G. S.; Daves, C. A.; Mann, K. R. *Inorg. Chem.* **1988**, *27*, 3347-3353.
(5) Milder, S. J.; Kliger, D. S. *J. Phys. Chem.* **1985**, *89*, 4170-4171.
(6) Milder, S. J. *Inorg. Chem.* **1984**, *24*, 3376-3378.
(7) Milder, S. J.; Kliger, D. S.; Butler, L. G.; Gray, H. B. *J. Phys. Chem.* **1986**, *90*, 5567-5570.
(8) Winkler, J. R.; Marshall, J. L.; Netzel, T. L.; Gray, H. B. *J. Am. Chem. Soc.* **1986**, *108*, 2263-2266.
(9) Marshall, J. L.; Stiegman, A. E.; Gray, H. B. in *Excited States and Reactive Intermediates*; Lever, A. B. P., Ed.; ACS Symposium Series 307; American Chemical Society: Washington, DC, 1986; pp 166-176.
(10) Mann, K. R.; Gordon, J. G., II.; Gray, H. B. *J. Am. Chem. Soc.* **1975**, *97*, 3553-3555.
(11) Mann, K. R.; Thich, J. A.; Bell, R. A.; Coyle, C. L.; Gray, H. B. *Inorg. Chem.* **1980**, *19*, 2462-2468.
(12) Smith, D. C. Ph.D. Thesis, California Institute of Technology, 1989.
(13) Miskowski, V. M.; Smith, T. P.; Loehr, T. M.; Gray, H. B. *J. Am. Chem. Soc.* **1985**, *107*, 7925-7934.
(14) Herde, J. L.; Lambert, J. C.; Senoff, C. V. *Inorg. Synth.* **1974**, *15*, 18-20.
(15) Green, M.; Kuck, T. A.; Taylor, S. H. *J. Chem. Soc. A* **1971**, 2334-2337.
(16) Robinson, S. D.; Shaw, B. L. *J. Chem. Soc.* **1965**, 4997-5001.

0002-7863/90/1512-3759$02.50/0

Table I. Crystal and Intensity Collection Data

formula: $Ir_2N_8C_{94}B_2H_{112}$	fw: 1772.03
crystal color: green	habit: flat plate
a = 17.678 (8) Å	α = 90°
b = 55.03 (4) Å	β = 110.54 (8)°
c = 18.01 (3) Å	γ = 90°
V = 16408 (8) Å^3	Z = 8
d_{calc} = 1.435 (1) g cm^{-3}	
λ = 0.71073 Å	room temperature
graphite monochromator	
space group: $P2_1/c$	absences: $h0l$, $l = 2n + 1$; $0k0$, $k = 2n + 1$
crystal size: 1.37 × 0.60 × 0.016 mm	μ = 34.88 cm^{-1}
CAD-4 diffractometer	θ–2θ scan, ω scan
2θ range: 0–18°	octants collected: $\pm h,k,l$
no. of reflcns meas: 1802	
no. of indep reflcns: 1505	
no. with $F_o^2 > 0$: 1381	
no. with $F_o^2 > 3\sigma(F_o^2)$: 1052	
goodness-of-fit for merging data: 1.51	

The IR spectra were taken on a Beckman IR 4240.

$[Ir_2(TMB)_4](PF_6)_2$. A filtered methanol solution of $NaPF_6$ was added to a stirred methanol solution of $[Ir_2(TMB)_4]Cl_2$ (prepared by the method of ref 13). Immediate precipitation of a blue powder occurred. The solution was filtered and the blue material recrystallized by slow evaporation of a toluene/acetonitrile solution. Electronic absorption spectra of this compound were identical with that of the $B(C_6H_5)_4^-$ salt except for the absence of absorption due to the $B(C_6H_5)_4^-$ anion in the UV region.

Ir(COD)(acac). A THF solution of Tl(acac) was added with stirring to a THF solution of $[Ir(COD)Cl]_2$. Formation of a white precipitate, TlCl, occurred immediately. The solution was stirred for approximately 1 h to ensure complete reaction. THF was removed under vacuum, and pentane was added. The solution was filtered through a Celite plug to yield a clear, bright yellow filtrate. The pentane was removed under vacuum to give a bright yellow crystalline material. The material was further purified by sublimation at 70–80 °C onto a water-cooled finger condenser (0 °C) at 10^{-5}–10^{-6} Torr. The final material was a bright yellow powder. Anal. Calcd for Ir(COD)(acac): C, 39.09; H, 4.79. Found: C, 38.3; H, 4.6. NMR: δ ($CDCl_3$, 20 °C) 1.60 (q, CH_2, 4 H), 1.98 (s, CH_3, 6 H), 2.23 (m, CH_2, 4 H), 3.93 (m, CH=CH, 4 H), 5.49 (s, CH, 1 H). This preparative method appeared to yield a product that was less contaminated with chloride impurities than the literature preparation.

$[Ir(CN\text{-}t\text{-}Bu)_4]BF_4$. To a clear yellow CH_3CN solution of $[Ir(COD)_2]BF_4$ was added, via syringe, a large excess of *tert*-butyl isocyanide (CN-*t*-Bu). A rapid color change from yellow to orange was observed. The solution was stirred for approximately 1 h. The solvent and volatiles were then removed under high vacuum, yielding an extremely air-sensitive bright orange solid.

Acetonitrile in this preparation was distilled twice from CaH_2, degassed with a minimum of five freeze–pump–thaw cycles, and stored under vacuum over activated alumina. The *tert*-butyl isocyanide was thoroughly degassed by five freeze–pump–thaw cycles. The reaction was done in a Vacuum Atmospheres inert atmosphere box to ensure oxygen exclusion. Earlier attempts to prepare the desired compound with standard Schlenk techniques produced materials that appeared to be partially oxidized according to UV–vis spectroscopic criteria. Attempts to prepare $Ir(CN\text{-}t\text{-}Bu)_4^+$ directly from $[Ir(COD)Cl]_2$ yielded material that did not give reproducible spectra. We infer that partial oxidation of the material is enhanced by chloride. NMR δ (CD_3CN, 20 °C): 2.49 (s, CH_3). IR (Nujol mull, NaCl plates): 2190 cm^{-1} (ν(CN), vs).

X-ray Data Collection and Reduction for $[Ir_2(TMB)_4][B(C_6H_5)_4]_2\cdot CH_3C_6H_5$. Crystal data are given in Table I. The thin flat-plate crystal was of a form suited for spectroscopic measurements, but ill-suited for X-ray diffraction. It was glued on a glass fiber with the c axis approximately parallel to the fiber. The b axis is perpendicular to the plate. The crystal was much larger than the collimator; it was centered on a Nonius CAD-4 diffractometer equipped with graphite-monochromated Mo Kα radiation. Unit cell dimensions were obtained from the setting angles of 14 reflections with 8.4° < 2θ < 10.1°; the long b axis caused difficulties in indexing the reflections. A data set of 1654 reflections in $\pm h,k,l$ out to 9° in 2θ was collected in a θ–2θ scan at 8°/min and then a second set of 148 data with h and k = 0 or 1 was collected with an ω scan. The θ–2θ data near the b axis were deleted and the two data sets merged. The data were corrected for absorption, and Lorentz and polarization factors were applied. The four independent iridium atoms were located from the Patterson map and their positions refined with six cycles of least squares (Table II). A subsequent Fourier map did not have sufficient resolution to locate the atoms of the TMB ligands, so refinement was terminated.

Table II. Coordinates of the Iridium Atoms

atom	x	y	z
Ir1	0.4155 (16)	0.1059 (5)	0.0742 (16)
Ir2	0.4828 (15)	0.1168 (5)	0.2580 (16)
Ir3	0.9180 (15)	0.1293 (5)	0.5440 (15)
Ir4	0.9659 (15)	0.1447 (5)	0.7277 (16)

Calculations were done with programs of the CRYM crystallographic computing system and ORTEP. Scattering factors and corrections for anomalous scattering were taken from a standard reference.[17] The function minimized in least squares was $\sum w(F_o^2 - F_c^2)^2$, where $w = 1/\sigma^2(F_o^2)$. Variances of the individual reflections were assigned on the basis of counting statistics plus an additional term, $(0.14)I^2$. Variances of the merged reflections were determined by standard propagation of error plus an additional term, $0.14 < I^2$. The absorption correction was done by Gaussian integration over an 8 × 8 × 8 grid. Transmission factors varied from 0.151 to 0.945.

Spectroscopic Measurements. All solvents were dried and degassed by standard methods.[18,19] Absorption spectra presented in Figures 2 and 6–9 were recorded with a Cary 17 spectrophotometer. Absorption and MCD spectra presented in Figures 4 and 5 were determined simultaneously along the same light path by means of a computer-controlled spectrometer described previously.[20] A field strength of 7.0 T was provided by a superconducting magnet system (Oxford Instruments SM2-7, fitted with a bore tube held at room temperature). The $\Delta\epsilon_M$ values are presented (M^{-1} cm^{-1} T^{-1}), where T is the magnetic field strength in Tesla units. All spectra were corrected for solvent blank. Single-crystal-polarized absorption measurements employed dual Glan–Thompson air-spaced calcite polarizers. Low-temperature absorption experiments were performed with two temperature control systems: a quartz optical Dewar of local design (77 K measurements) or a CTI-Cryogenics Model 70 Cryodyne Cryocooler. Propionitrile/2-MeTHF (1:2 volume ratio) solutions for 77 K glassy matrix experiments were prepared on a high-vacuum line in an evacuable 1-cm path length quartz cuvette attached to a high-vacuum Teflon stopcock.

Absorption spectra at ~20 K were recorded of single crystals mounted on quartz flats. Crystal orientation was established with a polarizing microscope; the crystals transmitted yellow-green and dark blue light for polarizations parallel to their two extinction directions determined between crossed polarizers. The former extinction was found to correspond to $\|a$ of the (010) crystal face. The extinctions were very sharp with white light and are, therefore, inferred to be wavelength independent in the visible region. The crystals were carefully masked with heat-conducting grease (fine copper powder suspended in vacuum grease) in order to provide good thermal contact with the cold station of the cryostat. The thickness of the $[Ir_2(TMB)_4][B(C_6H_5)_4]_2$ crystal whose spectra are given in Figures 7 and 8 was determined to be 21 μm with a micrometer. The thickness of the crystal whose spectra are shown in Figure 9 was not determined.

Results and Discussion

Crystal Structure of $[Ir_2(TMB)_4][B(C_6H_5)_4]_2\cdot CH_3C_6H_5$. In the course of our studies, we required thin single crystals for spectroscopic purposes. The crystal structure of $[Ir_2(TMB)_4][B(C_6H_5)_4]_2\cdot 2CH_3CN$, which had been determined previously,[12] revealed a cation orientation amenable to polarized spectroscopy, but crystals obtained from CH_3CN solution were chunky blue blocks, far too thick for spectroscopy. Attempts to grow thin crystals eventually yielded clusters of thin blue-green plates[21] by slow evaporation of toluene/acetonitrile solutions, from which high-quality spectroscopic data were obtained. X-ray examination of these crystals showed them not to be isomorphous with those of the structurally characterized material. NMR spectra showed

(17) *International Tables for X-ray Crystallography*; Kynoch Press: Birmingham, 1974; Vol. IV, pp 71, 149.

(18) Gordon, A. J.; Ford, R. A. *The Chemist's Companion*; John Wiley & Sons: New York, 1972.

(19) Perrin, D. D.; Armarego, W. L. F.; Perrin, D. R. *Purification of Laboratory Chemicals*; Pergamon: Oxford, 1966.

(20) Mason, W. R. *Anal. Chem.* **1982**, *54*, 646–648.

(21) The differences in color of the two phases are due to the high degree of orientation in the well-developed crystal face of the toluene solvate, one extinction (perpendicular to the Ir_2 axis) transmitting yellow-green light (see the Experimental Section). The crystals are air-stable when dry for days, but are air-oxidized (with notable surface degradation) upon longer exposure.

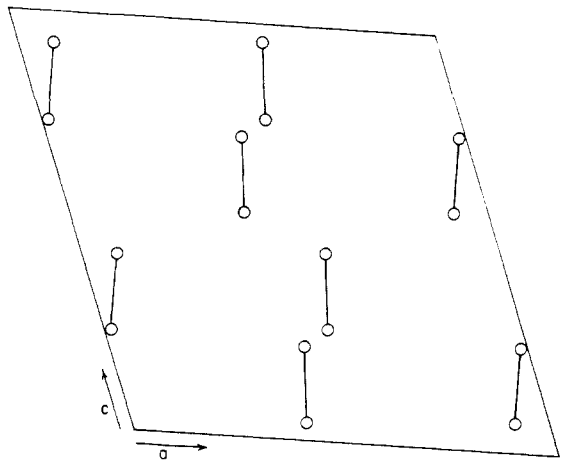

Figure 1. Projection of Ir–Ir units onto the (010) plane. Ir position indicated by O. The two metal atoms of a dimer unit are connected by a solid line.

that these crystals contained toluene ($n \approx 1$) instead of the acetonitrile of crystallization that was found in the previously characterized phase.[12,22]

The structure of this phase was partially determined, as described in the Experimental Section. The well-developed crystal face was (010); in Figure 1, we show a (010) view of the Ir–Ir units of the structure. The Ir_2 bond distances of the two independent Ir_2 units in this structure (3.16 (4) and 3.23 (4) Å) are, within their large esd, equivalent to those found in the earlier study, 3.199 (1) Å.[12] The Ir_2 units are all aligned nearly perpendicular to the *a* axis, which corresponds to an optical extinction, and lie very nearly in the (010) plane. Thus, our single-crystal-polarized spectra should approximate molecular *z* and *x,y* spectra for the $\perp a$ and $\parallel a$ polarizations, respectively. It should be noted that, for a monoclinic crystal face that does not contain the *b* axis, extinctions are not required to be parallel to a crystallographic axis nor are they required to be wavelength independent. However, both properties were found (within experimental error).

Electronic Spectrum of Ir(CN-*t*-Bu)$_4^+$. For comparison to binuclear Ir(I) complexes, it is important to have a reliable monomer electronic absorption spectrum. This apparently simple task proved to be difficult. We eventually obtained reproducible spectra for Ir(CN-*t*-Bu)$_4^+$ when a synthetic route (see the Experimental Section) was employed that rigorously excluded both halide and oxygen. The isolated BF_4^- salt is remarkably air-sensitive, instantaneously changing color from orange to blue green upon exposure to trace contamination of air. The probable explanation of this color change is the formation of partially oxidized oligomers,[23-29] analogous to well-characterized rhodium species such as $Rh_4b_8^{6+}$, which have similar colors.[23-25]

Well-characterized rhodium(I) isocyanide oligomeric systems, which are relatively air-insensitive, hence easier to handle, are thermally labile (because of very weak ground-state Rh–Rh bonding) but not photosensitive, since the excited states are strongly bound.[1,30,31] In contrast, partially oxidized rhodium(I) isocyanide oligomers are thermally much less labile (the Rh–Rh ground state is strongly bound) but undergo dissociative photochemistry.[23] Moreover, net photoreduction has been noted for rhodium isocyanide systems.[13] With regard to authentic Ir(I) oligomers, we note that samples of [Ir(CN-*t*-Bu)$_4$]BF_4 during dissolution in CH_3CN show flashes of blue-green color near the dissolving crystals, the color disappearing with diffusion into the bulk solvent. This may represent Ir(I) oligomerization in very concentrated solutions,[27] as previously reported for rhodium(I) isocyanides including the *tert*-butyl isocyanide complex.[31] We have not attempted to quantify this observation, however, because of the extreme difficulties involved in working with this compound.

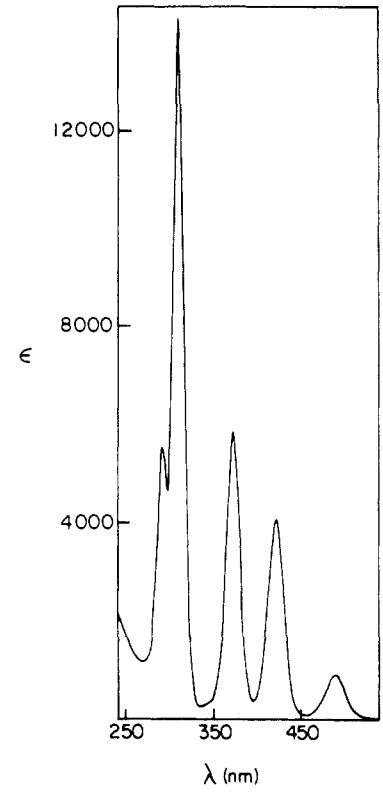

Figure 2. Electronic absorption spectrum of [Ir(CN-*t*-Bu)$_4$]BF_4 in CH_3CN at 25 °C.

Table III. Absorption Spectral Data for [Ir(CN-*t*-Bu)$_4$]BF_4 in CH_3CN at 25 °C

$^1A_{1g} \rightarrow$	λ_{max}, nm (ϵ, M^{-1} cm^{-1})	fwhm,[a] cm^{-1}
$E_u(^3A_{2u})$, $d_{z^2} \rightarrow p_z$	489 (870)	1130
$A_{2u}(^1A_{2u})$, $d_{z^2} \rightarrow p_z$	423 (4100)	1120
$E_u(^3E_u)$, $d_{xz,yz} \rightarrow p_z$	373 (5900)	1300
$E_u(^1E_u)$, $d_{xz,yz} \rightarrow p_z$	308 (14 500)	1360
$E_u(^3B_{1u})$, $d_{xy} \rightarrow p_z$	291 (5500)	*b*

[a] fwhm = full width at half the maximum height. [b] Not measured.

The electronic absorption spectrum of [Ir(CN-*t*-Bu)$_4$]BF_4 in dilute solution is shown in Figure 2; data are summarized in Table III. The observed bands are assigned to $d_{z^2} \rightarrow p_z$, $d_{xz,yz} \rightarrow p_z$, and $d_{xy} \rightarrow p_z$ excitations, in accord with the conventional MO scheme for square-planar d^8 complexes containing π-backbonding ligands.[28,31-34] The filled d level ordering is $d_{z^2} > d_{xz,yz} > d_{xy}$, and no electronic transitions involving the empty $d_{x^2-y^2}$ orbital have been assigned unambiguously for Rh(I) and Ir(I) complexes. As

(22) Determined from the ratio of the integrated intensities of the toluene methyl resonance and aromatic proton resonances to the integrated intensities of the TMB resonances. A signal corresponding to the methyl resonance of CH_3CN was not seen for this material, in contrast to the well-defined signal observed for the CH_3CN solvate.

(23) Miskowski, V. M.; Sigal, I. S.; Mann, K. R.; Gray, H. B.; Milder, S. J.; Hammond, G. S.; Ryason, P. R. *J. Am. Chem. Soc.* **1979**, *101*, 4383–4385.

(24) Sigal, I. S.; Gray, H. B. *J. Am. Chem. Soc.* **1981**, *103*, 2220–2225.

(25) Miskowski, V. M.; Gray, H. B. *Inorg. Chem.* **1987**, *26*, 1108–1112.

(26) Such species probably were encountered in earlier studies of iridium(I) isocyanide complexes.[27-29] In particular, Geoffroy et al.[29] found that blue Ir species in solution could be photolyzed to generate monomeric iridium(I) isocyanide complexes; these blue materials most likely were partially oxidized Ir oligomers.

(27) Kwakami, K.; Hoga, M.-A.; Tanaka, T. *J. Organomet. Chem.* **1973**, *60*, 363–373.

(28) Isci, H.; Mason, W. R. *Inorg. Chem.* **1975**, *14*, 913–918.

(29) Geoffroy, G. L.; Bradley, M. G.; Kenny, M. E. *Inorg. Chem.* **1978**, *17*, 777–779.

(30) Miskowski, V. M.; Nobinger, G. L.; Kliger, D. S.; Hammond, G. S.; Lewis, N. S.; Mann, K. R.; Gray, H. B. *J. Am. Chem. Soc.* **1978**, *100*, 485–488.

(31) Mann, K. R.; Lewis, N. S.; Williams, R. M.; Gray, H. B.; Gordon, J. G., II. *Inorg. Chem.* **1978**, *17*, 828–834.

(32) Isci, H.; Mason, W. R. *Inorg. Chem.* **1975**, *14*, 905–912.

(33) Geoffroy, G. L.; Isci, H.; Litrenti, J.; Mason, W. R. *Inorg. Chem.* **1977**, *16*, 1950–1955.

(34) Brady, R.; Flynn, B. R.; Geoffroy, G. L.; Gray, H. B.; Peone, J., Jr.; Vaska, L. *Inorg. Chem.* **1976**, *15*, 1485–1488.

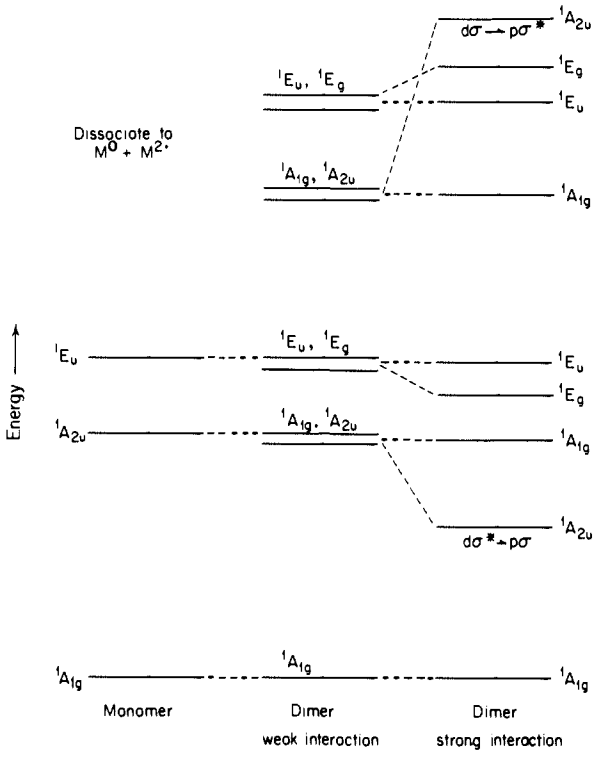

Figure 3. Qualitative VB state diagram for weak d/p interaction of two Rh(I) or Ir(I) monomers. Note that, for the strong interaction case, state energies are implicitly for the equilibrium bond distance of each individual state.

usual for such complexes, the last point only suggests the probable energetic ordering $d_{x^2-y^2} > p_z$ (i.e., that the LUMO is p_z), since d–d transitions to $d_{x^2-y^2}$ are dipole-forbidden and could be obscured by the intense (allowed) d → p absorptions.

The weak feature at 343 nm is not assigned. It could be a vibronic sideband involving one quantum of ν(CN) built upon $E_u(^3E_u)$, or it could represent a forbidden electronic transition.

Valence-Bond Model. Consider the electronic energy levels of a D_{4h} dimer in which one-electron coupling of the two centers is assumed to be zero. In this model, the single-center excitations are Davydov-coupled[35] in symmetric and antisymmetric fashion to yield dimer states. The low-lying dimer singlet states involving $d_{z^2} \rightarrow p_z$ and $d_{xz,yz} \rightarrow p_z$ excitations are shown in Figure 3.

There are four excited states correlating to $d_{z^2} \rightarrow p_z$ excitations. Two of these states ($^1A_{1g}$, $^1A_{2u}$) are derived from the $^1A_{2u}(d_{z^2} \rightarrow p_z)$ monomer excited state. In the VB picture, the remaining two excited states are a $^1A_{1g}$, $^1A_{2u}$ pair corresponding to excitation of a d_{z^2} electron on one center into a p_z orbital on the other center; thus, they are ionic states that must dissociate to M^{2+} plus M^0. As such, they must lie at much higher energy, even for no metal–metal bonding.

The energy of a metal-to-metal charge-transfer (MMCT) state is dependent on the ease of ionization of the metal center and the ability of a single metal center to accommodate an additional electron. Such a transition should scale roughly as $IP_d - EA_p$. An estimate of the molecular $IP_d - EA_p$ can be obtained by considering the atomic $IP_d - EA_p$. The atomic IP and EA values calculated for Rh and Ir are listed in Table IV.[36]

$$(d_{z^2})^2p_z^0 + (d_{z^2})^2p_z^0 \rightarrow (d_{z^2})^2p_z^1 + (d_{z^2})^1p_z^0$$

$$M^+ + M^+ \rightarrow M^0 + M^{2+}$$

The transition energies, as defined above, were corrected for $1/R$ (repulsion) terms (Table IV), but the molecular stabilization

Table IV. Metal-to-Metal Charge-Transfer Transition Energies

	calculated atomic state energy, hartrees		
	s^0d^8	p^1d^8	s^0d^7
Ir	−103.424 25	−103.541 44	−102.836 67
Rh	−108.362 42	−108.473 97	−107.738 84

	IP, eV	−EA, eV
Ir	15.99	−3.19
Rh	16.97	−3.03

	$M^+ + M^+ \rightarrow M^{2+} + M^0$		
	IP − EA, eV	(IP − EA) − $1/R$, eV	(IP − EA) − $1/R + S$,[a] eV
Ir	12.8	8.3	5.7 (45 000 cm^{-1})
Rh	13.9	9.4	6.8 (55 000 cm^{-1})

[a] S(molecular stabilization) = 2.6 eV.

of the atomic charge-transfer state (via delocalization of charge onto the ligands) has not been accounted for. An estimate of the molecular stabilization accompanying the MMCT can be obtained from earlier work on $Re_2Cl_8^{2-}$, a quadruply bonded ($\sigma^2\pi^4\delta^2$) metal dimer.[37] Similar to the binuclear d^8 complexes, the δ interaction is best viewed in the VB weak-coupling limit. Thus, $^1(\delta \rightarrow \delta^*)$ is an MMCT transition. It can be shown that the energy separation of the $^3(\delta\delta^*)$ (covalent) state and the $^1(\delta\delta^*)$ (ionic) state is $2K$[38]

$$K = \tfrac{1}{2}[(aa|aa) - (aa|bb)]$$

where (aa|aa) is the energy required to transfer a δ electron from metal center A to metal center B at infinite A–B distance. The (aa|bb) term is the electrostatic correction to finite R that we have already applied, as noted above. A value for the molecular stabilization of an MMCT state can be obtained by comparing the energy separation of the $^3(\delta\delta^*)$ and $^1(\delta\delta^*)$ excited states to the estimate based on atomic IP and EA values. For $Re_2Cl_8^{2-}$, the molecular stabilization of an MMCT state is 2.65 eV. This estimate was obtained with the use of the experimentally observed $^1(\delta\delta^*)$ transition energy[39] (which is greater than, but very close to, the singlet–triplet energy separation) and the calculated energy separation with ab initio atomic energies.[40]

With 2.6 eV as a rough estimate of the molecular stabilization of the charge-transfer state, MMCT energies for the Ir(I) and Rh(I) complexes are predicted to be in the UV with those of Ir lower than those of Rh (Table IV). These estimates are upper limits to the transition energies. The calculated IP and EA for Ir and Rh may be in error due to correlation effects not accounted for in the calculations. However, the excitation in question does not require increased pairing of electrons; therefore, energy differences (in particular, the predicted strong decrease in energy for Ir_2 versus Rh_2) may not have large errors associated with them.

The VB wave functions are equal mixtures of the two MO wave functions of the same symmetry. Thus, the two $^1A_{2u}$ wave functions are given by $d\sigma^*p\sigma \pm d\sigma p\sigma^*$, the plus combination corresponding to the lowest energy state. If we increase the metal–metal one-electron interaction (shorten the metal–metal

(35) Craig, D. P.; Walmsley, S. H. *Excitons in Molecular Crystals*; Benjamin: New York, 1968.

(36) Effective core potentials were utilized in which only the 19 outermost electrons of Rh and Ir are treated explicitly. See: Hay, P. J.; Wadt, W. R. *J. Chem. Phys.* **1985**, *82*, 299–310.

(37) Smith, D. C.; Goddard, W. A., III. *J. Am. Chem. Soc.* **1987**, *109*, 5580–5583.

(38) Hopkins, M. D.; Gray, H. B.; Miskowski, V. M. *Polyhedron* **1987**, *6*, 705–714.

(39) Cotton, F. A.; Walton, R. A. *Multiple Bonds Between Metal Atoms*; Wiley: New York, 1982.

(40) The calculated Re atomic spectrum was fit to the observed atomic spectrum with a Condon–Shortley formalism. Corrections to the Condon–Shortley parameters were determined so as to fit the calculated spectrum to the observed spectrum. These parameters were then used to correct the energies of other calculated Re atomic states:[12] Goodgame, M. M. Ph.D. Thesis, California Institute of Technology, 1984. The estimate of 2.65 eV is the difference between the observed $^1(\delta\delta^*)$ transition energy and the calculated value of 2K with the corrected atomic state energies. Using either the calculated $^3(\delta\delta^*)$ and $^1(\delta\delta^*)$ state splitting or the calculated $^1(\delta\delta^*)$ transition energy would require the use of uncorrected atomic-state energies and would not properly describe the ligand stabilization of the MMCT state.

distance), the two $^1A_{2u}$ states will mix in such a way as to resolve into the two MO wave functions, as indicated on the right-hand side of Figure 3.[41] Both the ^1E_u and $^1A_{1g}$ states are, at long distance, equal mixtures of bonding–bonding and antibonding–antibonding MO states; the $^1A_{1g}$ states, for example, are ($d\sigma^*p\sigma^* \pm d\sigma p\sigma$). Thus, bonding effects tend to cancel out. It is difficult to predict the relative bonding–antibonding contributions, particularly since the various interactions ($d\sigma$–$d\sigma$, $d\sigma$–$p\sigma$, $p\sigma$–$p\sigma$, $d\pi$–$d\pi$, etc.) undoubtedly maximize stabilization at greatly different metal–metal distances. However, it is reasonable that much less stabilization would arise than for $^1A_{2u}$ ($d\sigma^* \rightarrow p\sigma$), and our experimental data (vide infra) support the idea that the ^1E_u and $^1A_{1g}$ excitations are nearly vertical. There is, moreover, an interesting comparison available in diatomic mercury, Hg_2, which in its ground state ($s\sigma^2 s\sigma^{*2}$) is an extremely weakly bound van der Waals molecule.[42-44] Corresponding to the atomic $^1S \rightarrow {}^3P$ transition at 254 nm, Hg_2 shows two allowed transitions. One, $s\sigma^* \rightarrow p\sigma$, is to a strongly bound excited state and is richly structured in $\nu(Hg_2)$ and red-shifted from the atomic line. The second, ($s\sigma/s\sigma^*$) $\rightarrow$ ($p\pi/p\pi^*$), is vertical and shifted from the atomic line by only 57 cm^{-1}. These two Hg_2 states are clearly analogous to the low-lying $^1A_{2u}$ and ^1E_u excited states of d^8–d^8 Rh_2 and Ir_2 species.

Finally, we consider the ^1E_g excited states. The VB wave functions of these states ($d\pi^*p\sigma \pm d\pi p\sigma^*$) indicate that the lowest ^1E_g should be stabilized by resolving into the antibonding-to-bonding $d\pi^*p\sigma$ wave function. However, it is unclear how much stabilization can actually be expected, since $d\pi$ overlap will be very small except at short metal–metal distances, which would be precluded by repulsive metal–metal and ligand–ligand interactions. We compromise in Figure 3 by suggesting a smaller stabilization than for $^1A_{2u}$.

The important points that emerge from this discussion are that, in contrast to a simple MO picture, a VB model readily accommodates both weakly and strongly perturbed monomer transitions, and it identifies fully half of the dimer electronic excited states as ionic (MMCT); these ionic states should lie at considerably higher energy than the monomer excited states. These points prove to be crucial to understanding the electronic spectra of d^8–d^8 complexes.

Solution Electronic Absorption and MCD Spectra. The electronic absorption and MCD spectra of $Rh_2(TMB)_4^{2+}$ are shown in Figure 4. The assignments have been discussed extensively, with supporting single-crystal data,[1,11] and our present (entirely consistent) results are offered largely for comparisons with the Ir complex. Although the symmetry of the TMB complex is only D_4,[12] we will retain the g/u labels for ease of reference to the parent D_{4h} system (Figure 3).

The low-energy feature (λ_{max} 517 nm) is assigned to the $d\sigma^* \rightarrow p\sigma$ singlet [$A_{1g}(^1A_{1g}) \rightarrow A_{2u}(^1A_{2u})$] transition. This band shows the expected $-B$ term in the MCD spectrum.[45] The strong band centered at 314 nm is attributed to the $A_{1g}(^1A_{1g}) \rightarrow E_u(^1E_u)$ ($d\pi \rightarrow p\sigma$) excitation. This transition is to a degenerate excited state, and the MCD band appears to be dominated by a $+A$ term. A weak band (λ_{max} 340 nm) is observed to lower energy of the $E_u(^1E_u)$ band. From low-temperature polarized single-crystal spectra, this band is deconvoluted into two features,[1] an x,y-polarized component assigned to E_u of the ^3E_u transition (λ_{max} 342 nm) and a z-polarized A_{2u} component (λ_{max} 335 nm). The E_u component of the ^3E_u state should have $+A$ and $+B$ terms associated with it, and the A_{2u} state should exhibit a $-B$ term. Features attributable to transitions to the two ^3E_u states appear to be resolved in the MCD spectrum. A slight $-\Delta\epsilon$ is observed on the low-energy side of the MCD band at 330 nm ($\sim$3.0 μm^{-1}), indicating a weak $+A$ term; this transition is dominated by a $+B$ term. Similarly weak $+A$ terms have been observed for analogous states of monomeric rhodium(I) isocyanides.[28] To higher energy, a transition with a $-B$ term is observed, consistent with the presence of an A_{2u} state.

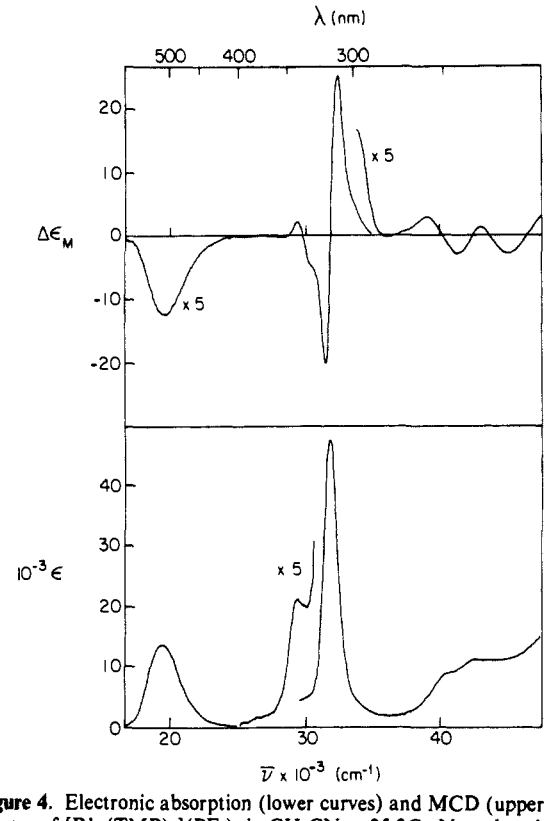

Figure 4. Electronic absorption (lower curves) and MCD (upper curves) spectra of $[Rh_2(TMB)_4](PF_6)_2$ in CH_3CN at 25 °C. Note that the MCD scales in the regions 210–295 and 400–600 nm have been expanded 5-fold; similarly, the absorptivity scale has been expanded 5-fold in the 325–400-nm region. $\Delta\epsilon_M$ has units of (M cm T)$^{-1}$.

Several weak features are observed to higher energy of the $E_u(^1E_u)$ transition. The shoulder at 290 nm appears to have a $+B$ term, in accord with an $E_u(^3B_{1u})d_{xy} \rightarrow p\sigma$ assignment. However, the feature could represent a vibronic $E_u(^1E_u) + \nu(CN)$ transition, and the energy and low intensity of the band are reasonable for either assignment. The two bands above 250 nm (4.00 μm^{-1}) appear to possess A terms, indicating degenerate excited states, although the interpretation of the data for the higher energy band is ambiguous. Emission polarization ratios of these bands measured for 77 K glassy solutions also are consistent with x,y-polarization, again most clearly for the lower energy band.[46] These bands have not been reported in previous work (largely because they are obscured by anion absorption for $B(C_6H_5)_4^-$ salts), but we note here that similar features are seen in the spectra of all other binuclear rhodium(I) isocyanide complexes that we have examined, whereas monomers such as $Rh(CN\text{-}t\text{-}Bu)_4^+$ show no resolved absorption in this region.[46] Assignments are given in Table V.

The electronic absorption and MCD spectra of $[Ir_2(TMB)_4](PF_6)_2$ are shown in Figure 5. In analogy to $Rh_2(TMB)_4^{2+}$, the intense absorption centered at 625 nm (ϵ 11 200 M^{-1} cm^{-1}) is assigned to the fully allowed $A_{1g}(^1A_{1g}) \rightarrow A_{2u}(^1A_{2u})$ ($d\sigma^* \rightarrow p\sigma$) excitation. This band shows the expected $-B$ term in the MCD. The intense features above 300 nm, with maxima at 318 (ϵ 22 000 M^{-1} cm^{-1}) and 372 nm (ϵ 9750 M^{-1} cm^{-1}), are attributed to $d\pi \rightarrow p\sigma$ transitions to $E_u(^1E_u)$ and $E_u(^3E_u)$ states, respectively. The 318-nm absorption, while complicated by the

(41) The higher energy $^1A_{2u}$ state ("$d\sigma \rightarrow p\sigma^*$") obviously does not demand a shorter metal–metal bond. However, its extreme antibonding character mandates a higher energy, as supported by calculations[43] on analogous states of Hg_2.

(42) Morse, M. D. *Chem. Rev.* **1986**, *86*, 1049–1109.
(43) Celestino, K. C.; Ermler, W. C. *J. Chem. Phys.* **1984**, *81*, 1872–1881.
(44) Zee, R. D. van; Blankespoor, S. C.; Zwier, T. S. *J. Chem. Phys.* **1988**, *88*, 4650–4654, and references therein.

(45) For a detailed description of MCD terms together with the theory and conventions in standard use, see: Piepho, S. B.; Schatz, P. N. *Group Theory in Spectroscopy with Application to Magnetic Circular Dichroism*; Wiley-Interscience: New York, 1983.

(46) Miskowski, V. M. Unpublished results.

Table V. Absorption Maxima for $Rh_2(TMB)_4^{2+}$ and $Ir_2(TMB)_4^{2+}$

$^1A_{1g} \rightarrow$	λ_{max}, nm (ϵ, M^{-1} cm^{-1}) [$\nu \times 10^{-3}$, cm^{-1}]	fwhm,[a] cm^{-1}	MCD $\nu \times 10^{-3}$, cm^{-1}	MCD $\Delta\epsilon_M$, M^{-1} cm^{-1} T^{-1}
	$[Rh_2(TMB)_4](PF_6)_2$ in CH_3CN (25 °C)			
$E_u(^3A_{2u})$, $d\sigma^* \rightarrow p\sigma$	[b]			
$^1A_{2u}$, $d\sigma^* \rightarrow p\sigma$	517 (13 600) [19.3]	2800	19.5	−2.45
$E_u(^3E_u)$, $d_{xz,yz} \rightarrow p_z$	340 (4200, sh) [29.4]		27.8 28.7 29.5	−0.076 0.0 +2.38
$A_{2u}(^3E_u)$, $d_{xz,yz} \rightarrow p_z$	[c]		30.4 (sh)	−4.67
$E_u(^1E_u)$, $d_{xz,yz} \rightarrow p_z$	314 (47 500) [31.8]	1400	31.5 31.9 32.4	−20.1 0.0 +25.2
$E_u(^3B_{1u})$, $d_{xy} \rightarrow p_z$ and/or $E_u(^1E_u)$ + ν(CN)	290 (3500, sh) [34.5]		~33 (sh)	~+5
MMCT(?)	245 (8600, sh) [40.8]		39.1 40.2 41.4	+0.59 0.0 −0.581
MMCT(?)	234 (10 700, sh) [42.7]		42.4 43.0 45.1	0.0 +0.291 −0.531
	$[Ir_2(TMB)_4][B(C_6H_5)_4]_2$ in CH_3CN (25 °C)[d]			
$^1A_{2u}$, $d\sigma^* \rightarrow p\sigma$	625 (11 200) [16.0]	2200	16.1	−1.26
$E_u(^3E_u)$, $d_{xz,yz} \rightarrow p_z$	372 (9750) [26.8]	1000	26.3 26.6 27.1	−0.118 0.0 +6.25
+ ν(CN)	[b]			
$A_{2u}(^3E_u)$, $d_{xz,yz} \rightarrow p_z$	333 (4000, sh) [30.1]		30.3	−12.0
$E_u(^1E_u)$, $d_{xz,yz} \rightarrow p_z$	318 (22 000) [31.3]	1300	30.9 (sh) 31.3 32.3	−10.1 0.0 +8.98
$E_u(^3B_{1u})$, $d_{xy} \rightarrow p_z$	305 (9500, sh) [32.8]		(obscured)	
MMCT				
$E_u(^3E_u)$, $d_{xz,yz} \rightarrow p_z$	~280 (8500, sh) [~36]		34.6 35.1 35.6	−1.05 0.0 +0.23
$E_u(^1E_u)$, $d_{xz,yz} \rightarrow p_z$	268 (17 000) [37.3]	1500	36.5 36.9 37.5	−1.34 0.0 +3.49
			38.8	−1.95
"$d\sigma \rightarrow p\sigma^*$"	~230 (25 000) [43.5]		43.1	−1.20

$[Ir_2(TMB)_4][B(C_6H_5)_4]_2$ in a Glassy Matrix of CH_3CH_2CN/2MeTHF (77 K)

$^1A_{1g} \rightarrow$	λ_{max}, nm (ϵ, M^{-1} cm^{-1})	fwhm,[a] cm^{-1}	$^1A_{1g} \rightarrow$	λ_{max}, nm (ϵ, M^{-1} cm^{-1})	fwhm,[a] cm^{-1}
$E_u(^3A_{2u})$, $d\sigma^* \rightarrow p\sigma$	820 (150)	1500	$E_u(^3B_{1u})$, $d_{xy} \rightarrow p_z$	304 (6000)	800
$^1A_{2u}$, $d\sigma^* \rightarrow p\sigma$	635 (25 500)	1200	MMCT		
$E_u(^3E_u)$, $d_{xz,yz} \rightarrow p_z$	373 (17 000)	650	$E_u(^3E_u)$, $d_{xz,yz} \rightarrow p_z$	280 (11 000, sh)	
+ ν(CN)	344 (1500, sh)		$E_u(^1E_u)$, $d_{xz,yz} \rightarrow p_z$	268 (32 000)	1000
$A_{2u}(^3E_u)$, $d_{xz,yz} \rightarrow p_z$	331 (5000)	700	"$d\sigma \rightarrow p\sigma^*$"	[e]	
$E_u(^1E_u)$, $d_{xz,yz} \rightarrow p_z$	320 (38 000)	690			

[a] fwhm = full width at half the maximum height. [b] Not observed. [c] Polarized single-crystal spectra resolve this band into two features: $E_u(^3E_u)$, λ_{max} 342 nm; $A_{2u}(^3E_u)$, λ_{max} 335 nm. [d] MCD data for PF_6^- salt. [e] Not determined because of anion absorption.

overlap of the weaker bands to low and high energy, displays the expected $+A$ term in the MCD. The $A_{1g}(^1A_{1g}) \rightarrow E_u(^3E_u)$ transition appears in the MCD as a skewed band due to the contribution of the $+A$ and $+B$ terms. In comparison to $Rh_2(TMB)_4^{2+}$, there is a much larger $+A$ term contributing to this transition.

A relatively weak absorption centered at 820 nm is observed in both single crystals and concentrated solutions. This band, whose MCD was not measured because of spectrometer limitations, is assigned to the $^3(d\sigma^* \rightarrow p\sigma)$ transition. Another relatively weak feature appears as a shoulder to lower energy of the 372-nm band. A similar (weak) absorption is found in the spectrum of $Rh_2(TMB)_4^{2+}$.

Shoulders are observed on both the high- (305 nm) and low-energy (333 nm) sides of the 318-nm band in the spectrum of $Ir_2(TMB)_4^{2+}$ (these features are not well resolved in the $Rh_2(TMB)_4^{2+}$ spectrum). The low-energy shoulder appears as a $-B$ term in the MCD spectrum, consistent with a transition to $A_{2u}(^3E_u)$. The shoulder to higher energy, although overlapped with the ^1E_u band, appears to be dominated by a $+B$ term, perhaps with a small $-A$ component, in accord with the $E_u(^3B_{1u})$ $d_{xy} \rightarrow p\sigma$ transition. In addition, bands to higher energy of 300 nm are resolved for both the $B(C_6H_5)_4^-$ and PF_6^- salts. None of these features has an analogue in monomer spectra. The two lower energy bands exhibit $+A$ terms in the MCD, indicating transitions to degenerate excited states. The highest energy shoulder possesses a weak $-B$ term and no A term, suggestive of a transition to a nondegenerate excited state. Assignments are listed in Table V.

The energies and widths of the bands derived from the lowest energy $d_{z^2} \rightarrow p_z$ excitation for $Ir_2(TMB)_4^{2+}$ differ strikingly from those associated with the $d_{z^2} \rightarrow p_z$ absorption in the spectrum of $Ir(CN\text{-}t\text{-}Bu)_4^+$. The smaller d–p gap and the greater widths of the $A_{2u}(^1A_{2u})$ and $E_u(^3A_{2u})$ bands are a consequence of the enhanced metal–metal-bonding interaction in the $^{1,3}(d\sigma^*p\sigma)$ excited states of the dimer. Promotion of an electron from $d\sigma^*$ to $p\sigma$ produces a large molecular distortion; this distortion is mainly a contraction along the metal–metal coordinate.[1]

In contrast to the $d\sigma^* \rightarrow p\sigma$ transition, features assigned to the $d\pi \rightarrow p\sigma$ excitation have energies and widths very similar to those observed for the monomer, implying very little if any molecular distortion along the metal–metal coordinate. If one adheres strictly to the MO model for the binuclear complex, a shift in the $d\sigma^*$

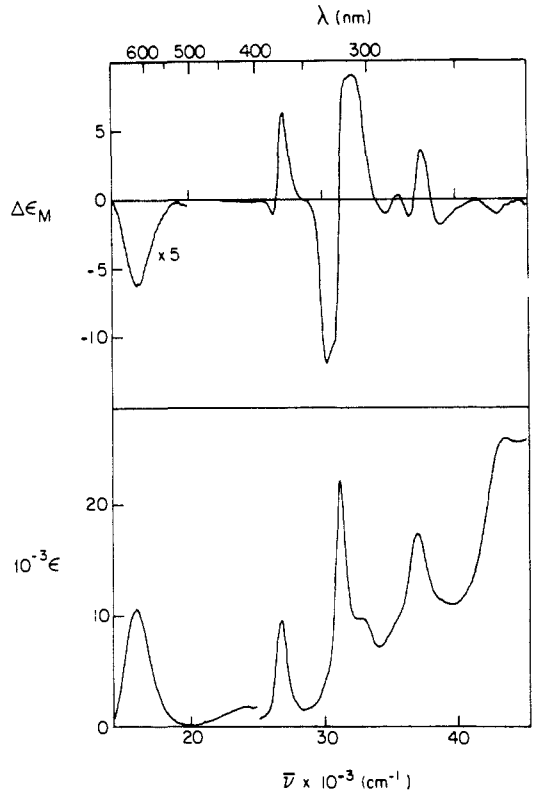

Figure 5. Electronic absorption (lower curve) and MCD (upper curves) spectra of $[Ir_2(TMB)_4](PF_6)_2$ in CH_3CN at 25 °C. Note that the MCD scale has been expanded 5-fold in the 500–700-nm region. $\Delta\epsilon_M$ has units of $(M\ cm\ T)^{-1}$.

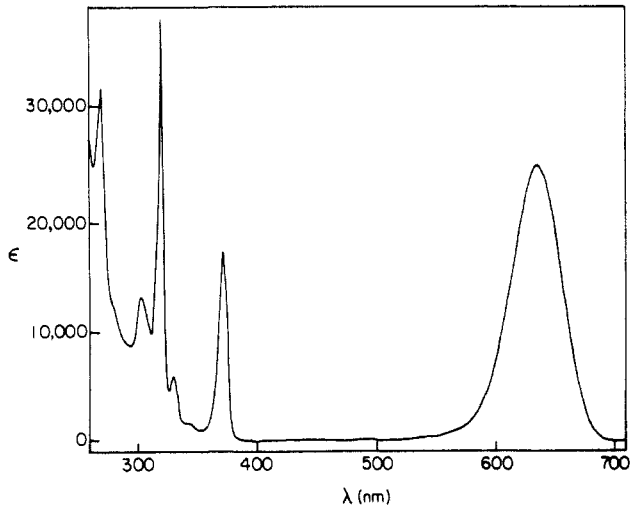

Figure 6. Electronic absorption spectrum of $[Ir_2(TMB)_4][B(C_6H_5)_4]_2$ in a glassy matrix of CH_3CH_2CN/2-MeTHF (1:2 volume ratio) at 77 K.

→ pσ transitions implies a shift in the dπ → pσ excitations, unless pσ/dσ and pσ/pσ bonding interactions are negligible,[1] which would contradict the ground-state bonding picture. Since a large shift is observed for the dσ* → pσ transitions and very little if any shift is seen for dπ → pσ, the VB model is preferred; according to VB, the low-energy dσ* → pσ transition is red-shifted from the monomer $d_{z^2} \rightarrow p_z$ due to a favorable metal–metal interaction at shorter distance, with the $^{1,3}E$ states only slightly shifted from their reference monomer energies.

The weak features observed to lower energy of the $A_{1g}(^1A_{1g}) \rightarrow E_u(^3E_u)$ transition have been the subject of much speculation. Arguments against assignments to transitions to $d_{x^2-y^2}$ derived levels (e.g., ligand-field excited states) have been presented, and other assignments have been suggested, $d_{xy} \rightarrow p_z$, dσ* → pσ*, and dσ → pσ.[1]

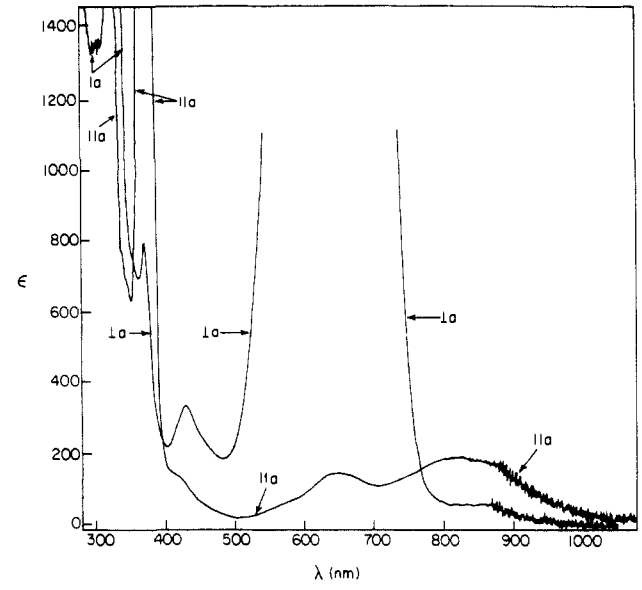

Figure 7. Polarized single-crystal absorption spectra of $[Ir_2(TMB)_4][B(C_6H_5)_4]_2$ at 25 °C. The ∥a base line is vertically offset by 20ε units.

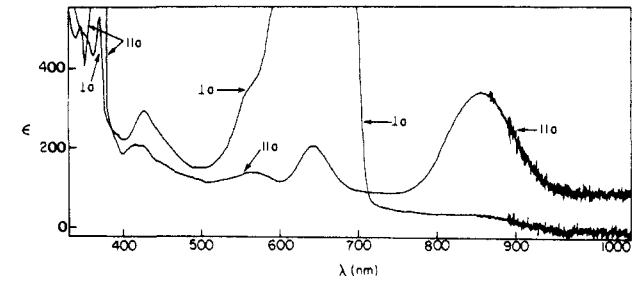

Figure 8. Polarized single-crystal absorption spectra of $[Ir_2(TMB)_4][B(C_6H_5)_4]_2$ at 24 K. The ∥a base line is vertically offset by 100ε units.

Figure 6 shows the low-temperature (77 K) absorption spectrum of $[Ir_2(TMB)_4][B(C_6H_5)_4]_2$. Upon cooling, the expected sharpening and red shifting of $A_{1g}(^1A_g) \rightarrow A_{2u}(^1A_{2u})$ (dσ* → pσ) are observed. The red shift of the maximum indicates that the effective vibrational frequency that is coupled to the electronic transition is higher in the excited state than in the ground state.[47]

The high-energy portion of the spectrum resolves impressively upon cooling. The bands assigned to dπ → pσ excitations sharpen but do not shift. The shoulders on each side of the 320-nm band are resolved into distinct features with widths similar to those of the intense dπ → pσ absorptions. A weak shoulder at 344 nm attributable to one quantum of ν(CN) (2260 cm^{-1}) built on $E_u(^3E_u)$ is resolved. The similarity of the high-energy portion of the low-temperature absorption spectrum of $Ir_2(TMB)_4^{2+}$ to that of $Ir(CN\text{-}t\text{-}Bu)_4^+$ is remarkable.

Single-Crystal-Polarized Spectra of $[Ir_2(TMB)_4][B(C_6H_5)_4]_2 \cdot CH_3C_6H_5$. The room-temperature polarized single-crystal absorption spectra of $[Ir_2(TMB)_4][B(C_6H_5)_4]_2 \cdot CH_3C_6H_5$ are shown in Figure 7. The $A_{1g}(^1A_{1g}) \rightarrow A_{2u}(^1A_{2u})$ band (λ_{max} 645 nm) shows the expected z polarization (⊥a in this lattice). At lower energy is the x,y-polarized $A_{1g}(^1A_{1g}) \rightarrow E_u(^3A_{2u})$ band (λ_{max} 830 nm). These two features are the dσ* → pσ transitions.

After the sample is cooled to 24 K, the spectrum sharpens and reveals additional features not resolved at room temperature (Figure 8). To the high-energy side of the $A_{2u}(^1A_{2u})$ band, a feature assignable to one quantum of ν(CN) (2100 cm^{-1}) is observed in both polarizations (λ_{max} 568 nm). (Modes of e_g and a_{1g} symmetries presumably lead to ⊥z and ∥a intensities, respectively.) This feature appears as a broad shoulder in the x,y-polarized room-temperature spectrum. The weak absorption at 642 nm in the ∥a spectra at both room temperature and 24 K is

(47) Ballhausen, C. J. *Molecular Electronic Structures of Transition Metal Complexes*; McGraw-Hill: New York, 1979; pp 132–135.

Table VI. Polarized Single-Crystal Spectra of $[Ir_2(TMB)_4][B(C_6H_5)_4]_2$

	25 °C			24 K		
$^1A_{1g} \rightarrow$	pol	λ_{max}, nm (ϵ, M^{-1} cm^{-1})	fwhm, cm^{-1}	pol	λ_{max}, nm (ϵ, M^{-1} cm^{-1})	fwhm, cm^{-1}
$E_u(^3A_{2u})$, $d\sigma^* \rightarrow p\sigma$	x, y	830 (180, $\|a$; 60, $\perp a$)	2200	x, y	855 (250, $\|a$; 40, $\perp a$)	1300
$^1A_{2u}$, $d\sigma^* \rightarrow p\sigma$	z	645 (140, $\|a$; $\perp a$[a])		z	642 (110, $\|a$; $\perp a$[a])	1100
$+ \nu$(CN)	z; x, y	565		z; x, y	568 (50, $\|a$)	
b	x, y	~455 (40 sh, $\|a$)		x, y	~450 (65 sh, $\|a$)	
$^1A_{1g}$, $d\sigma/\sigma^* \rightarrow p\sigma/\sigma^*$	$z > x, y$	430 (~300, $\perp a$)	1400	$z > x, y$	428 (300, $\perp a$)	1500
b				x, y	415	
$E_u(^3E_u)$, $d_{xz,yz} \rightarrow p_z$	x, y	371		x, y	369	
$+ \nu$(CN)	z; x, y	345 (sh)		z; x, y	344	
$A_{2u}(^3E_u)$, $d_{xz,yz} \rightarrow p_z$	z	~328				
$E_u(^1E_u)$, $d_{xz,yz} \rightarrow p_z$	x, y	>320				

[a] Off-scale. [b] Not assigned; see text.

interpreted in terms of a vibronically induced $\perp z$ component of the transition to $A_{2u}(^1A_{2u})$, presumably involving low-frequency modes of e_g symmetry.[48] The observation that the intensity of this feature decreases significantly as the temperature is reduced to 24 K is consistent with the vibronic interpretation. The band assigned to the transition to $E_u(^3A_{2u})$ sharpens and red shifts, as expected due to the higher frequency metal–metal vibration in the excited state. Similar to the $A_{1g}(^1A_{1g}) \rightarrow E_u(^3A_{2u})$ band in the spectrum of $Rh_2(TMB)_4^{2+}$, but in contrast to $Rh_2b_4^{2+}$, no vibronic structure is resolved at 24 K.[1] The metal–metal vibration (which is known from a Raman study of the Ir_2 complex to have values of 55 and 132 cm^{-1} in the ground and $^3A_{2u}$ excited states, respectively)[49] is expected to be the primary promoting mode for this electronic transition. The absence of a resolved $\nu(M_2)$ vibronic progression built on the electronic absorption band may be due to broadening attributable to vibronic coupling involving a low-energy ligand mode.

Several well-resolved bands are observed to higher energy of the $d\sigma^* \rightarrow p\sigma$ absorption. The intense feature at 369 nm displays x,y-polarization, as expected for the $A_{1g}(^1A_{1g}) \rightarrow E_u(^3E_u)$ system. The weak band at 344 nm, resolved in both room-temperature and 24 K spectra, is x,y-polarized; it represents one quantum of a_{1g} ν(CN) (1970 cm^{-1}) built on the transition to $E_u(^3E_u)$. The sharp band at 369 nm in the z-polarized spectrum also is assigned to $A_{1g}(^1A_{1g}) \rightarrow E_u(^3E_u)$; it appears in this polarization because of the slight misalignment of the chromophore in the crystal. The shoulder to higher energy is a transition to $E_u(^3E_u)$ plus one quantum of ν(CN), presumably an e_g mode in this polarization.

Unambiguous polarizations for the higher energy transitions could not be obtained because available crystals were too thick to allow maxima to be measured in either polarization. Indirect polarizations were obtained from the room-temperature spectra (Figure 7), which could be extended to higher optical density than the low-temperature spectra. The band at 328 nm appears to be z polarized, since intensity in the $\perp a$ polarization goes off scale near 340 nm, well before it does in the $\|a$ polarization, but then comes back on scale at ~318 nm. This polarization is consistent with the $A_{1g}(^1A_{1g}) \rightarrow A_{2u}(^3E_u)$ assignment. The intense bands to higher energy are similarly indicated to be x,y-polarized, since the absorption $\perp a$ remains on scale down to nearly 290 nm. These observations are consistent with our assignments of the intense solution bands at 318 and 305 nm as the x,y-polarized transitions $A_{1g}(^1A_{1g}) \rightarrow E_u(^1E_u)$ and $A_{1g}(^1A_{1g}) \rightarrow E_u(^3B_{1u})$.

Several weak features are resolved to lower energy of the $A_{1g}(^1A_{1g}) \rightarrow E_u(^3E_u)$ band. The weak absorptions in the 400–500-nm region are better resolved and show distinct polarizations in low-temperature single-crystal spectra of a thicker crystal of $[Ir_2(TMB)_4][B(C_6H_5)_4]_2 \cdot CH_3C_6H_5$ (Figure 9). Similar features have been reported for the analogous Rh complex.[1] Because of drastic thermal narrowing of the intense bands to higher and lower energy (Figures 7 and 8), the temperature dependence of the intensity of these bands is obscured. The most intense band, which peaks at 428 nm, is predominantly z polarized. In x,y polarization,

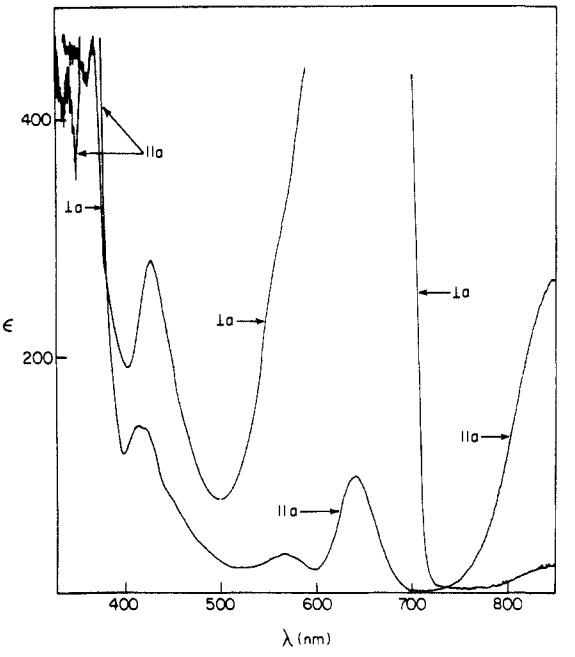

Figure 9. Polarized absorption spectra of a relatively thick crystal of $[Ir_2(TMB)_4][B(C_6H_5)_4]_2$ at 22 K.

the shape of the absorption is reproducibly very different, and we infer additional weak shoulders at 415 and 450 nm. The absorption maxima and other data extracted from the polarized single-crystal spectra of $[Ir_2(TMB)_4][B(C_6H_5)_4]_2$ are set out in Table VI.

Interpretation of the weak features to the red of the $A_{1g}(^1A_{1g}) \rightarrow E_u(^3E_u)$ band has presented a problem. One initially attractive assignment, suggested for Rh_2 complexes, was to excitation into the $d\sigma^*$ (Rh–C) orbitals derived from $Rh(d_{x^2-y^2})$,[50] as excited states of this type have been postulated to be thermally accessible from $^3A_{2u}(d\sigma^* \rightarrow p\sigma)$.[51] However, the half-widths of these bands are far too narrow for transitions to $d_{x^2-y^2}$ derived orbitals, because the excited state in question would be strongly distorted along ν(M–C) coordinates.

The $d_{xy} \rightarrow p_z$ transitions ($d\delta$, $\delta^* \rightarrow p\sigma$), which are dipole-forbidden for both mononuclear and binuclear d^8 complexes, were viewed as another candidate for the weak features.[1] The assignment of the 291-nm band in the spectrum of $[Ir(CN\text{-}t\text{-}Bu)_4]BF_4$ to a transition to $E_u(^3B_{1g})$ (derived from $d_{xy} \rightarrow p_z$) indicates that it is not likely that the weak feature at 430 nm in $Ir_2(TMB)_4^{2+}$ represents an analogous excitation. The $d_{xy} \rightarrow p_z$ transitions evidently are only weakly perturbed, as are the $d_{xz,yz} \rightarrow p_z$ excitations.

Another possibility is that $d\sigma \rightarrow p\sigma$ and $d\sigma^* \rightarrow p\sigma^*$ excitations[1] are responsible for the 428-nm band. (The relevant excited state, $d\sigma^*p\sigma^* + d\sigma p\sigma$, may not be strongly bound (vide infra) and,

(48) The intensity is too high, according to oriented gas calculations, to be attributable to the slight misorientation of the Ir_2 axes.
(49) Dallinger, R. F.; Smith, D. C. Unpublished results.
(50) Rice, S. F. Ph.D. Thesis, California Institute of Technology, 1982.
(51) Rice, S. F.; Milder, S. J.; Gray, H. B.; Goldbeck, R. A.; Kliger, D. S. *Coord. Chem. Rev.* **1982**, *43*, 349–354.

therefore, is best described as an excited monomer weakly coupled to a ground-state monomer.) The spectral bandwidth (1500 cm^{-1}) is too great to correspond to a $d\pi \rightarrow p\sigma$ transition, but it is similar to the bandwidths associated with $d_{z^2} \rightarrow p_z$ excitations. Such transitions are dipole-forbidden; hence, the absorptions should be weak, with intensities induced by vibronic or crystal site symmetry couplings. An interesting consequence of such an assignment is the correspondence of the 428-nm band in the spectrum of $Ir_2(TMB)_4^{2+}$ to the $A_{1g}(^1A_{1g}) \rightarrow A_{2u}(^1A_{2u})$ ($d_{z^2} \rightarrow p_z$) absorption at 423 nm in $Ir(CN\text{-}t\text{-}Bu)_4^+$. A similar correspondence between dimer and monomer band positions has been noted previously for the $d\pi \rightarrow p_z$ and $d_{xy} \rightarrow p_z$ excitations.

Only one transition to $^1A_{1g}(d_{z^2} \rightarrow p_z)$ is expected near 430 nm, since the other one (MO model) is to an ionic state in the VB model (Figure 3). Possible assignments for the additional weak features near 430 nm are transitions to $^{1,3}E_g$ bound states arising from $d\pi/\pi^* \rightarrow p\sigma/\sigma^*$ excitations. Such features might be somewhat red shifted from the monomer transitions and have widths comparable to the bound $d\sigma^* \rightarrow p\sigma$ excitation. The low intensities would suggest spin-forbidden transitions, possibly $^3(d\pi/\pi^* \rightarrow p\sigma/\sigma^*)$.

If the $d\sigma/\sigma^* \rightarrow p\sigma/\sigma^*$ assignment is correct for $Ir_2(TMB)_4^{2+}$, a corresponding band should be observed for the analogous Rh complexes. Indeed, for $Rh_2(TMB)_4^{2+}$ and $Rh_2b_4^{2+}$, bands at 375 and 385 nm, respectively, are resolved, each with the appropriate width and polarization.[46] (The transition to $A_{2u}(^1A_{2u})$ in the spectrum of $Rh(CNEt)_4^+$ is observed at 380 nm.)[28]

High-Energy Features. The MMCT transitions for Ir(I) and Rh(I) are estimated to appear at approximately 240 and 200 nm, respectively. These estimates indicate that the broad features below 300 nm in the spectra of $Ir_2(TMB)_4^{2+}$ (280 and 268 nm) and $Rh_2(TMB)_4^{2+}$ (245 and 234 nm) could be MMCT. The *A*-term behavior in the MCD spectrum suggests transitions to $^{1,3}E_u(d_{xz,yz} \rightarrow p_z)$ states. The peak separation observed for $Ir_2(TMB)_4^{2+}$ (1300 cm^{-1}) is consistent with the expected singlet–triplet state splitting. For the covalent $d_{xz,yz} \rightarrow p_z$ transition, peak separations of 1200 cm^{-1} [$E_u(^1E_u)$ to $A_{2u}(^3E_u)$] and 4500 cm^{-1} [$E_u(^1E_u)$ to $E_u(^3E_u)$] are found. The large bandwidths are attributed to ligand distortions caused by the change in electron density around the metal. In analogy to $Ir_2(TMB)_4^{2+}$, the high-energy features for $Rh_2(TMB)_4^{2+}$ are tentatively assigned to MMCT ($d_{xz,yz} \rightarrow p_z$) transitions. While this is but one of the possible assignments (others are MLCT or transitions to $d_{x^2-y^2}$ states, which would have to be from $d\pi/\pi^*$ levels in order to account for the *A* terms), the large blue shift of the bands on going from Ir to Rh is consistent with the ionic nature of the transitions and not obviously in accord with any other interpretation. In line with this discussion, the highest energy band for $Ir_2(TMB)_4^{2+}$, which shows a weak $-B$ term, may represent a transition to an ionic $^1A_{2u}$ state derived from $d\sigma/\sigma^* \rightarrow p\sigma/\sigma^*$ (e.g., the $d\sigma \rightarrow p\sigma^*$ state of the MO limit).

Conclusions

The MO model accounts for many important aspects of the metal–metal interactions in binuclear d^8 complexes, but it is unable to accommodate all of the observed spectral features. The VB model allows for dimer transitions that are highly perturbed from the monomer bands, as well as monomer-like dimer excitations. The VB model also identifies half of the dimer electronic excited states as ionic, involving metal-to-metal charge transfer; these MMCT states do not correlate to any monomer states. With the VB model, we have been able to rationalize the energies and widths of the previously observed bands; in addition, we have arrived at plausible assignments for bands that were either not interpreted satisfactorily or not observed in earlier work.

There is a striking similarity of our picture of the d^8–d^8 states to that derived from the spectroscopy of van der Waals molecules. The VB model does not change any of the MO-based interpretations of the thermal chemistry, photochemistry, or photophysics of these systems. What it does do is emphasize that weakly bound ground-state systems will show just a few strongly stabilized excited states that correlate to monomer states, and these are the only ones that MO theory describes correctly. The weakly perturbed monomer-like states and, particularly, the ionic states, are better described by the VB model.

Acknowledgment. We thank Bill Schaefer, Terry Smith, Steve Rice, Dave Brinza, Bill Goddard, and Woody Woodruff for many helpful discussions. D.C.S. acknowledges a graduate fellowship from the Sun Co. This research was supported by National Science Foundation Grant CHE84-19828.

Registry No. $[Ir_2(TMB)_4](PF_6)_2$, 125713-77-1; Ir(COD)(acac), 12154-84-6; $[Ir(CN\text{-}t\text{-}Bu)_4]BF_4$, 125686-71-7; $[Ir_2(TMB)_4][B(C_6H_5)_4]_2{\cdot}CH_3C_6H_5$, 125713-78-2; $Rh_2(TMB)_4^{2+}$, 73367-41-6.